Using stable Mg isotope signatures to assess the fate of magnesium during the *in situ* mineralisation of CO_2 and H_2S at the CarbFix site in SW-Iceland

Eric H. Oelkers[1,2,3], Rhiannon Butcher[3], Philip A.E. Pogge von Strandmann[3], Jan A. Schuessler[4], Friedhelm von Blankenburg[4], Sandra Ó. Snæbjörnsdóttir[1,5], Kiflom Mesfin[1], Edda Sif Aradóttir[5], Ingvi Gunnarsson[5], Bergur Sigfússon [5], Einar Gunnlaugsson[5], Juerg M. Matter[6,7], Martin Stute[7], Sigurdur R. Gislason[1]

[1]*Institute of Earth Science, University of Iceland, Iceland*
[2]*CNRS/UMR 5563, Université Paul Sabatier, France*
[3]*London Geochemistry and Isotope Centre (LOGIC), University College London and Birkbeck, University of London, Gower Place, London, UK.*
[4]*GFZ German Research Centre for Geosciences, Telegrafenberg, 14473 Potsdam, Germany*
[5]*Reykjavik Energy, Iceland*
[6]*Ocean and Earth Science, University of Southampton, UK*
[7]*Lamont-Doherty Earth Observatory, Columbia University, USA*

Abstract - The *in-situ* carbonation of basaltic rocks could provide a long-term carbon storage solution. To investigate the viability of this carbon storage solution, 175 tonnes of pure CO_2 and 73 tonnes of a 75% CO_2-24% H_2S-1% H_2-gas mixture were sequentially injected into basaltic rocks as a dissolved aqueous fluid at the CarbFix site at Hellisheidi, SW-Iceland. This paper reports the Mg stable isotope compositions of sub-surface fluids sampled prior to, during, and after the CO_2 injections. These Mg isotopic compositions are used to trace the fate of this element during the subsurface carbonation of basalts. The measured Mg isotopic compositions of the monitoring well fluids are isotopically lighter than the dissolving basalts and continue to become increasingly lighter for at least two years after the gas-charged water injection was stopped. The results indicate that the formation of isotopically heavy Mg-clays rather than Mg-carbonates are the predominant Mg secondary phases precipitating from the sampled fluids. Isotope mass balance calculations suggest that more than 70% of the Mg liberated from the basalt by the injected gas charged water was precipitated as Mg-clays, with this percentage increasing with time after the injection, consistent with the continued precipitation of Mg clays over

the whole of the study period. The formation of Mg clays in response to the injection of CO_2 into basalts, as indicated in this study, could be detrimental to carbon storage efforts because the formation of these minerals consume divalent Mg that could otherwise be used for the formation of carbonate minerals and because such clays could decrease host rock permeability.

1. Introduction

The CarbFix project was created to develop the technology to store carbon dioxide as stable carbonate minerals directly in the subsurface by reacting gas charged injection waters with basaltic rocks (Gislason et al., 2010, 2018; Aradóttir et al., 2011, 2018). Carbon storage in basaltic rocks offers numerous advantages including their ability to promote mineral carbonation and their large potential storage volume (McGrail et al., 2006; Goldberg and Slagle, 2009; Goldberg et al., 2010; Gislason and Oelkers, 2014; Snæbjörnsdóttir et al., 2014). As such, numerous studies have focused on developing the technology to safely store CO_2 in basaltic rocks including laboratory (Assayag et al., 2009; Flaathen et al., 2009; Gudbrandsson et al., 2011; Stockmann et al., 2011; Gysi and Stefánsson, 2012; Rosenbauer et al., 2012; Galeczka et al., 2014; Mareni et al., 2018), modelling (McGrail et al., 2006; Van Pham et al., 2012; Goldberg et al., 2009, 2013; Rosenbauer et al., 2012; Bacon et al., 2014) and field efforts (Rogers et al., 2006; Matter et al., 2007; McGrail et al., 2011, 2012; Siggfusson et al., 2015). Basaltic rocks are rich in divalent cations such as Ca^{2+}, Mg^{2+}, and Fe^{2+}. The injection of acidic CO_2-charged water promotes the release of these metals, potentially leading to the formation of carbonate minerals such as calcite, magnesite, and siderite as the continued dissolution of basalt increases the pH of the aqueous fluid (Oelkers et al., 2008; Gislason et al., 2010, 2014; Stefánsson et al., 2011; Gislason and Oelkers, 2014; Olsson et al., 2014). About 5% of the continents and most of the oceanic floor are comprised of basaltic rocks, including the mid-oceanic ridges. As such the largest basaltic storage potential lies offshore; theoretically all CO_2 from the burning of fossil fuel carbon (estimated to be ~5000 Gt; Archer, 2005) could be stored by mineral carbonation along the mid-ocean ridges (Snæbjörnsdóttir et al., 2014). The flanks of these ridges contain highly fractured and permeable basaltic layers (Fisher, 1998) with a pervasive circulation of about 1,000 Gt

69 seawater/yr (Harris and Chapman, 2004). The potential for using these marine systems
70 for carbon storage is confirmed by the results of Wolff-Boenisch et al. (2011), who
71 demonstrated the rapid dissolution of basaltic rocks in CO_2 charged seawater.
72
73 The efficiency of mineral carbonation, however, can be limited if Mg clay minerals
74 rather than Mg carbonate minerals form in response to the injection of CO_2 into basalts.
75 Magnesium clay formation is detrimental to carbon storage efforts because these minerals
76 consume divalent Mg that could otherwise be used for the carbonate mineral formation,
77 and because Mg-bearing clays could decrease host rock permeability. The fate of Mg
78 during mineral carbonation efforts in basalts will be assessed in this study through the
79 application of Mg isotopes. The stable isotopes of magnesium (^{24}Mg, ^{25}Mg and ^{26}Mg)
80 are increasingly being used as tracers of geochemical processes, including their use to
81 assess mineral reactions during weathering (Brenot et al., 2008; Huang et al., 2012; Liu et
82 al., 2014; Pogge von Strandmann et al., 2012; Tipper et al., 2006, 2008, 2012a, 2012b;
83 Wimpenny et al., 2011). Like all major elements, magnesium and its isotopes are affected
84 by a number of processes. For example, the magnitude and sign of Mg isotope
85 fractionation during precipitation appears to be dependent on the type of mineral forming
86 (Geske et al., 2012; 2015; Immenhauser et al., 2010; Li et al., 2012, 2015; Saulnier et al.,
87 2012; Wombacher et al., 2011), organic vs. inorganic precipitation (Chang et al., 2004;
88 Pogge von Strandmann, 2008; Saenger and Wang, 2014), precipitation rate (Mavromatis
89 et al., 2013), fractionation mechanism (Buhl et al., 2007), and aqueous speciation (Li et
90 al., 2014; Schott et al., 2016). In addition, isotopic fractionation can also occur due to
91 both the preferential incorporation and preferential adsorption of specific Mg isotopes
92 (Huang et al., 2012; Liu et al., 2014; Opfergelt et al., 2011; Pogge von Strandmann et al.,
93 2008, 2012; Tipper et al., 2012a; Wimpenny et al., 2010, 2014). Finally, the uptake of
94 Mg by plants and microbes causes variable isotope fractionation (Black et al., 2006;
95 Bolou-Bi et al., 2010, 2012; Oelkers et al., 2015; Pokharel et al., 2017; Uhlig et al.,
96 2017).
97
98 In this study the Mg isotope systematics of subsurface fluids sampled prior to, during,
99 and after the injection of CO_2-charged waters into subsurface basalts was measured to

provide insight into the mineralisation reactions that occurred in response to this injection. This approach takes advantage of the distinct Mg isotope fractionation signatures of primary and secondary phases. The Mg isotope ratio of primary igneous silicate rocks is virtually uniform (Teng et al., 2010a; Pogge von Strandmann et al., 2011) and it differs markedly from that in carbonates (Chang et al., 2004; Pogge von Strandmann, 2008; Wombacher et al., 2011; Li et al., 2012, 2014; Saenger and Wang, 2014, Teng 2017). As such, the Mg isotope composition of surface waters is often controlled by the balance of dissolution of silicate to carbonate rocks in the host catchment and/or the relative precipitation rates of Mg-clays compared to Mg-bearing carbonates (Tipper et al., 2006a, 2006b, 2008; Pogge von Strandmann et al., 2008, 2014). It is thus anticipated that a similar approach will provide insight into the identity of Mg minerals formed during subsurface processes occurring at the CarbFix site.

2. Background of the CarbFix Project

This study focuses on the fate of Mg liberated from dissolving basalts in response to the injection of CO_2-charged water at the CarbFix injection site. A number of past publications have reported the details of this injection, including the temporal evolution of dissolved element compositions and chemical tracers following these injections. A description of the injection method was presented by Sigfússon et al. (2015). The temporal evolution of chemical tracers, dissolved carbon and pH in the first monitoring well downstream from the injection well was reported by Matter et al. (2016), as well as an estimate of the fraction of injected carbon fixed by carbonation reactions. This study concluded that more than 95% of the dissolved carbon injected into the subsurface was fixed as stable carbonate minerals within 2 years. The concentrations of dissolved major elements during and after injection in the first monitoring well, as well as the saturation indices of potential secondary minerals were described by Snæbjörnsdóttir et al. (2017). Reaction path modelling of the carbon dioxide charged injection fluids, as they reacted with the subsurface basalts were reported by Snæbjörnsdóttir et al. (2018).

The CarbFix injection site is equipped with a 2000 m deep injection well and 8

monitoring wells ranging in depth from 50 to 1300 m in depth. The subsurface rocks at the injection site are primarily olivine tholeiite basalts consisting of lava flows and hyaloclastite formations (see Fig. 1). The hyaloclastites are relatively low permeability glassy rocks formed under ice and melt water during glaciations; the boundaries between hyaloclastites and lava flows, and those between individual lava flows boundaries are preferential fluid flow pathways (Alfredsson et al., 2013). Some alteration is observed in the hyaloclastite rocks starting at 120 to 300 m depth. The common alteration minerals at this depth are smectite, calcite, Ca-rich zeolites, and poorly crystalline iron-hydroxides (Alfredsson et al., 2013). Fluid injection was targeted at a lava flow sequence located 400–800 m below the surface with the main aquifer located at ~530 m depth. Loss on ignition measurements on rock samples suggest that over 80% of the primary rocks in the target zone are currently unaltered. Tracer tests were conducted both under natural and forced flow conditions from 2008 to 2011 to define the system hydrology (Aradóttir et al., 2012; Gislason et al., 2010; Khalilabad et al., 2008). These tests indicated that the flow from the HN-02 injection well to the first monitoring well (HN-04) consists of relatively homogenous porous media intersected by a low volume and fast flow path that channels about 3% of the tracer flow (Khalilabad et al., 2008).

The water in the target zone prior to the injection ranged in temperature from 15 to 35 °C and had *in situ* pH ranging from 8.4 to 9.8. The concentrations of dissolved CO_2 and O_2 collected from the injection well from the target reservoir were 1.27×10^{-3} and 1.1×10^{-5} mol/kg, respectively, prior to the injection (Alfredsson et al., 2013). These values are substantially undersaturated with respect to the composition of these gases in the atmosphere, suggesting that the target injection reservoir was isolated from the surface. The concentration of Ca and Mg in these waters prior to the injection was limited by secondary mineral precipitation (Alfredsson et al., 2013). All the water samples collected from the target reservoir prior to the injection of CO_2 charged water were supersaturated with respect to Ca-zeolite, analcime, Ca–Mg–Fe smectite, calcite, and aragonite, and some are supersaturated with respect to dolomite and Fe–Mg carbonates (Snæbjörnsdóttir et al., 2017).

Approximately 175 tons of pure commercial CO_2 and 73 tons of a 75%–24%–0.8% mixture of CO_2–H_2S–H_2 gases were dissolved into water during their injection from January until August 2012. This latter gas mixture was captured directly from the adjoining Hellisheidi power plant by its dissolution into water at elevated pressure (Gislason et al., 2018; Sigfusson et al., 2018). The injected water had a temperature of ~25 °C and was equilibrated with 26 to 28 bars pressure of the CO_2 gas or ~14 bars pressure of the CO_2–H_2S–H_2 mixture. The injected fluid equilibrated with pure carbon dioxide had dissolved CO_2 concentrations of ~0.8 mol/kg H_2O and a pH of 3.85, whereas the fluid equilibrated with the gas mixture had a dissolved CO_2 concentration of ~0.43 mol/kg H_2O and a pH of 4.0 (Snæbjörnsdóttir et al., 2017). All host rock minerals and glass were strongly undersaturated with respect to the gas charged injection waters (Snæbjörnsdóttir et al., 2018). The interaction of these acidic fluids with the host basalts creates porosity near the injection well by dissolving primary and secondary minerals. As gas-charged water continues to dissolve the basaltic host rock, this fluid becomes increasingly basic and secondary minerals will precipitate, potentially clogging the system. Reaction path calculations reported by Snæbjörnsdóttir et al. (2018) suggested that Mg–Fe–carbonates and siderite became supersaturated in the subsurface fluids at pH <5, whereas Ca-Mg-Fe-carbonates and calcite were saturated or supersaturated at higher pH. Mg bearing clays and Ca, Na-rich zeolites also became saturated in the subsurface fluids at pH >7.

3. Sampling and Analytical Methods

A detailed overview of fluid injection and sampling before, during and after the CarbFix injections have been reported by Snæbjörnsdóttir et al. (2017). Sampling of the fluids from the HN-04 monitoring well and other wells surrounding the injection well began in 2008. Water samples for chemical analysis were collected several times prior to the injections, which began during January 2012 (Alfredsson et al., 2013). During the injections and until mid-September 2012 the HN-04 injection well was sampled twice weekly. Weekly sampling continued until mid-July 2013 with few exceptions. Water was

pumped from this monitoring well at the rate of 3.5 m^3/h throughout this study maintaining a constant head from the injection to the monitoring well.

Fluid samples were collected via a 10 m long, 10 mm diameter stainless steel pipe connected to the 53 mm diameter monitoring well lining pipe extending down to the pump (Alfredsson et al., 2016). The sample pipe was connected directly to a sampling valve inside an on-site field laboratory. After flushing the sampling pipe, the sampled waters were immediately filtered through 0.2 μm Millipore cellulose acetate membranes using silicon tubing and a 140 mm Sartorius® filter holder. All air in the filtration system was expelled through a valve prior to sampling and at least 3 L of water was pumped through the system before the samples were collected in acid washed high density polyethylene bottles for cation and isotopic analysis. The sampling bottles were also washed with the monitoring well fluids three times before the final sampling. These samples were acidified using Suprapur® HNO_3, 1% (v/v) then stored prior to analysis. The fluid sample Si, Ca, Mg concentrations, alkalinity and pH data used in this study were previously reported by Snæbjörnsdóttir et al. (2017) and Alfredsson et al. (2013). Four pre-CO_2-injection fluid samples from different shallow wells and 19 post-injection monitoring well (HN-04) samples were selected for Mg isotope measurements (Table 1). Samples collected prior to the acid gas injections from the deep wells (> 400 m), including the HN-04 monitoring well, could not be analysed for their Mg isotopic ratios due to their low Mg concentrations (see Fig. 2). These concentrations did not exceed 6 μmol kg^{-1} (Alfredsson et al., 2013; Snæbjörnsdóttir, et al., 2017).

Mg isotope analyses - Prior to stable Mg isotope analyses, the fluid samples were chemically purified by cation exchange chromatography in a clean laboratory equipped with filtered air laminar flow workstations at GET Toulouse following a protocol similar to that reported by Mavromatis et al. (2012, 2013), Pearce et al. (2012), and Shirokova et al. (2013). Briefly, fluid samples were evaporated to dryness and re-dissolved in 1M HNO_3 prior to loading onto 10 ml Bio-Rad poly-prop columns containing AG-50W-X12 resin (200–400 mesh) for separation of Mg from other elements. A total of 23 samples were processed in two batches of Mg column chemistry. With each batch of samples, the

IAPSO seawater reference material and a procedure blank was processed for quality control. Mg recovery after chromatographic separation was >99.5%. After column chemistry, samples were evaporated, treated with H_2O_2/HNO_3 at 150°C to remove any remaining organics, and finally re-dissolved in 0.3M HNO_3.

Mg isotope measurements were performed at the HELGES lab, GFZ Potsdam, following protocols described by Uhlig et al. (2017) and Pokharel et al. (2017). Before Mg isotope ratio analysis, the purity of the Mg sample solutions and the Mg content in procedure blanks were checked by ICP-OES (Varian 720ES) and quadrupole ICP-MS (Thermo iCAP-Qc), respectively. Most of the samples showed a purity of higher than 99% Mg; for some samples that did not, we tested that the remaining impurities of Na and K would cause no analytical bias. Doping DSM-3 with Na and K and measuring the Mg isotopic composition showed that the impurities did not bias the Mg isotope measurements, i.e., the Na-K-doped DSM-3 ($\delta^{26}Mg$ = -0.05±0.10 ‰, 2SD) was identical to pure DSM-3 within analytical uncertainty, consistent with previous findings (Pokharel et al., 2017). Procedural blanks contributed less than 0.9% to the Mg processed through column chemistry (15 µg) and are therefore considered insignificant (potential bias in $\delta^{26}Mg$ is less than 0.04 ‰). All Mg isotope ratio measurements were performed in medium resolution mode on a Thermo Neptune multi-collector inductively coupled plasma mass spectrometer (MC-ICP-MS). Samples and the DSM3 bracketing standard were diluted in 0.3 M HNO_3 to 500 ppb. The solutions were introduced to the MC-ICP-MS via a quartz-glass spray chamber (double pass cyclon-scott type, Thermo SIS) equipped with a self-aspirating ca. 100 µL/min. The Mg isotope signals ($^{24}Mg^+$, $^{25}Mg^+$, $^{26}Mg^+$) were measured simultaneously on Faraday detectors. ^{26}Mg was measured on the interference-free low mass side of the flat-top peak to avoid interference from $^{12}C^{14}N^+$. Sample signal intensities of ca. 12 V for $^{24}Mg^+$ were obtained. Background intensities (< 8 mV $^{24}Mg^+$) were measured on-peak in 0.3 M HNO_3 before and after each sample measurement block and were subtracted from sample signal intensities. Instrumental mass bias on measured Mg isotope ratios was corrected by the sample-standard bracketing method using concentration-matched DSM3 as a standard.

253 We report isotope ratios of samples as per mil deviation of the $^{26}Mg/^{24}Mg$ and
254 $^{25}Mg/^{24}Mg$ ratios from the DSM3 international reference material using the delta
255 notation, as $\delta^{26}Mg$ and $\delta^{25}Mg$, respectively. All results are consistent with mass
256 dependent isotope fractionation. Average δ-values obtained from 2 to 6 replicate
257 measurements of the same fluid are reported in Table 1 together with twice the standard
258 deviation (2SD), which indicates the instrument repeatability. To assess total analysis
259 uncertainty, IAPSO Atlantic seawater was also analysed with our samples and gave a
260 mean $\delta^{26}Mg$ of -0.90±0.08 (n = 12), which is in agreement with literature reference values
261 (-0.83 ±0.09 ‰, 2SD, Foster et al. 2010, Ling et al. 2011 and references therein). The
262 pure Mg solution Cambridge-1 was measured 21 times during this study and gave a $\delta^{26}Mg$
263 of -2.62±0.10‰ (2SD), which is also in close agreement with literature values (-2.59 to
264 2.78‰ – see compilations by Pogge von Strandmann et al., 2011; An and Huang, 2014).
265 These observations are consistent with previously established long-term uncertainty
266 estimates of the MC-ICP-MS method at GFZ HELGES of ±0.06‰ (2SD) for $\delta^{25}Mg$ and
267 ±0.10‰ (2SD) for $\delta^{26}Mg$ (Uhlig et al., 2017; Pokharel et al., 2017).
268

269 ## 4. Results

270 The Mg isotope compositions of four pre-injection shallow well samples,
271 collected during 2008 and 2010 from wells HK-12, HK-13, and HK-25, which are drilled
272 to depths of 130, 210 and 310 m, respectively, are shown in Fig. 3, and listed in Table 1;
273 the composition of selected elements in these fluids are provided in Table 2. The
274 measured $\delta^{26}Mg$of these samples ranged from -0.57 to -0.69 ‰, which is ~0.3‰ lower
275 than basaltic rocks from this area and previously measured groundwaters in Iceland
276 (Pogge von Strandmann et al., 2008), but within the range of precipitation-uncorrected
277 Icelandic soil pore waters (Pogge von Strandmann et al., 2012). Note that the formation
278 of Mg-bearing clays in these systems occurs only at depths greater that 120 to 300 m
279 (Alfredsson et al., 2013), such that these shallow water samples are likely relatively
280 unaffected by Mg clay precipitation compared to deeper wells, which is also consistent
281 with the relatively high Mg concentrations of these fluids.
282

The fluid compositions of the HN-04 monitoring well fluids are provided in Tables 1 and 2. The first of these samples analysed for δ^{26}Mg was collected on 9 February 2012, 17 days after the start of the initial CO_2-charged water injection. This sample had a Mg concentration of 36 μmol kg^{-1} and a δ^{26}Mg of -0.84 ‰, which is approximately 0.25 ‰ lower than that of the pre-injection shallow well samples. As the aqueous Mg concentrations of the monitoring well fluids increased with time up to 101 μmol kg^{-1} on 26 March 2012 (Fig. 2b) the δ^{26}Mg values of these fluids decreased to -0.94 ‰. These δ^{26}Mg values continued to decrease with time to about -1.3 ‰ through June 2013 as the dissolved Mg concentration decreased, increased, and decreased again in response to the arrival to the monitoring well of fluids influenced by the injection of the acid gases (see Fig. 2, 3). The isotopically lightest δ^{26}Mg value of -1.34 ‰ was measured in the final sample collected on 8 June 2014.

5. Discussion

The basaltic glass in the region of CarbFix injection site has a δ^{26}Mg value of -0.28‰ (Pogge von Strandmann et al., 2008; Wimpenny et al., 2010), which is identical to State University of New York (SUNY) Mid-Ocean Ridge Basalt (MORB; Teng et al., 2007), as well as the bulk silicate Earth (Hin et al., 2017). This glass is susceptible to dissolution in response to the injection of acidic fluids (Gislason et al, 1996; Oelkers, 2001; Oelkers and Gislason, 2001; Gislason and Oelkers, 2003) and has been identified as the major phase dissolving in response to the CarbFix gas charged water injections (Snæbjörnsdóttir et al., 2018). The rapid fluid-flow pathway, channeling ~3% of the injected gas charged fluid was attributed to a fracture network located in crystalline basalts containing mainly plagioclase, olivine, and pyroxene. Nevertheless olivines and crystalline basalts near the CarbFix site have an identical δ^{26}Mg composition to each other and the basaltic glass (Pogge von Strandmann et al., 2008, 2012). This is consistent with other studies suggesting basaltic olivines have a narrow isotopic range, with a similar Mg isotope composition to that of its coexisting basalt glass (Norman et al., 2006; Teng et al., 2007; Wimpenny et al., 2010; Liu et al., 2017). Although such results indicate that the preferential dissolution of distinct primary phases will not cause significant Mg isotope fractionation, it should be noted that both Wimpenny et al. (2010)

and Maher et al. (2016) reported an initial preferential loss of light Mg during the dissolution of basaltic glass and olivine. Longer-term experiments reported by Oelkers et al. (2015) however, suggest that for the case of olivine, this preferential release of light Mg is limited to the initial stages of dissolution.

The low Mg concentrations in the target reservoir fluids prior to the gas injection indicate that essentially all the Mg dissolved in the HN-04 monitoring well samples collected in this study after January 2012 originates from the injected fluids or the dissolution of the host minerals in response to fluid-rock interaction. The low Mg concentrations of the target reservoir prior to injection have been attributed to the formation of Mg-bearing secondary minerals in the subsurface reservoirs, and in particular to Mg-bearing clay precipitation. Indeed, the smectite, Mg-saponite, is calculated to be strongly supersaturated in these fluids prior to injection, whereas dolomite and magnesite are undersaturated (Snæbjörnsdóttir, et al., 2017). These calculated results are consistent with the observed secondary minerals in the target basalt formations (Alfredsson et al., 2013). They also explain the low δ^{26}Mg of the pre-injection shallow reservoir fluids compared to that of the host basalt, as Mg-bearing silicate minerals preferentially incorporate heavy Mg isotopes upon their formation (c.f. Young and Galy, 2004; Tipper et al., 2006; Teng et al., 2007, 2010; Pogge von Strandmann et al., 2008).

It seems likely, therefore, that the increasingly isotopically light composition of the post-injection well samples must either be caused by continued dissolution of an isotopically light and previously formed secondary phase, or the precipitation of an isotopically heavy secondary phase. Evidence suggests the calcite present in the host basalts dissolve as the acidic gas charged injection waters first interact with the subsurface basalts (Snæbjörnsdóttir et al., 2017). This calcite likely has a δ^{26}Mg of no more than -1.4‰ (Saenger and Wang 2014; Wombacher et al., 2011) such that the initial dissolution of calcite would tend to make the fluids lighter. Nevertheless, after a short initial time, saturation state and reactive path calculations indicate that calcite, as well as dolomite and mixed Mg-Ca-Fe carbonates, become supersaturated in the monitoring

345 fluids collected from the HN-4 monitoring well (Snæbjörnsdóttir et al., 2017, 2018). The
346 initially dissolved calcite tends to precipitate from this fluid as its pH increases in
347 response to basalt dissolution. Due to the injection of carbon dioxide, more calcite
348 precipitates in this system than it initially dissolved (Matter et al., 2016; Snæbjörnsdóttir
349 et al., 2018). Such carbonate minerals likely tend to preferentially incorporate light Mg
350 into their structure. For example, Mavromatis et al. (2014) found that apparent dolomite-
351 pore fluid δ^{26}Mg fractionation factors were -2.6 ‰, a value similar to that reported by
352 Higgins and Schrag (2010). Numerous other studies have observed the preferential
353 incorporation of light Mg in Mg-bearing carbonates (Galy et al., 2002; Buhl et al., 2007;
354 Hippler et al., 2009; Immenhauser et al., 2010; Wombacher et al., 2011; Li et al., 2012,
355 2015; Pearce et al., 2012; Mavromatis et al., 2012, 2013; Shirokova et al., 2013; Beinlich
356 et al., 2014; Prikryl et al., 2018). Such observations suggests that carbonate precipitation
357 as observed at the CarbFix site would drive the sampled monitoring well to heavier rather
358 than lighter compositions. It seems therefore that carbonate precipitation is not the
359 dominant process controlling the Mg isotope composition of these monitoring well fluids.
360
361 The measured formation water composition requires, therefore, the incorporation
362 of heavy Mg into secondary phases. The calculations reported by Snæbjörnsdóttir et al.
363 (2017, 2018) suggest that Mg-smectites are supersaturated in most of the monitoring
364 fluids collected from the HN-4 monitoring well; the saturation state of the monitoring
365 fluids analyzed in this study with respect to Mg-clay are provided in Table 2. The Mg
366 isotopic compositions of clay minerals tend to be heavier than their co-exisiting fluid
367 phases (Young and Galy, 2004; Tipper et al., 2006; Teng et al., 2007, 2010; Pogge von
368 Strandmann et al., 2008). Similarly, Wimpenny et al. (2010) concluded that the formation
369 of secondary chrysotile, an Mg clay, lead to light Mg release from dissolving basaltic
370 glass and olivine. Ryu et al. (2016) estimated a clay-fluid Mg isotope fractionation factor
371 of 0.54 ‰, for T-O-T clays formed at temperatures from 90 to 250 ^{o}C. Moreover,
372 Wimpenny et al. (2014) measured the brucite-fluid δ^{26}Mg fractionation factor to be
373 0.50‰ at 80 ^{o}C and near to neutral pH. This study argued that this system provided a
374 good analogue to the incorporation of Mg into the octahedral sheets of Mg-rich clay
375 minerals. Note also that ^{26}Mg preferentially adsorbs on the surfaces of kaolinite type

minerals, including allophane (Huang et al., 2012; Pogge von Strandmann, 2012; Opfergelt et al., 2014). Thus, both precipitation and adsorption of exchangeable Mg onto clay minerals could lead to the observed pore fluid $\delta^{26}Mg$ decrease with time.

If, to a first approximation, it can be assumed that the Mg isotopic composition of the HN-04 monitoring fluids stem exclusively from the conservative dissolution of basalt[1] having an isotopic composition of $\delta^{26}Mg_{basalt}$ = -0.28‰ (Pogge von Strandmann et al., 2008), coupled to the precipitation of a Mg-clay having a $\Delta^{26}Mg_{clay\text{-}fluid}$ fractionation factor of 0.50‰ (Wimpenny et al., 2014), the fraction of Mg released to the fluid by the basalt and originally injected into the well with the gas charged fluid that was incorporated into clays can be estimated from mass balance constraints. The Mg concentration of the sampled monitoring well fluids is equal to the sum of contributions from the Mg concentration of the injected gas charged water ($c_{Mg,inject}$), the Mg concentration of the original formation water ($c_{Mg,fw}$), and the change in Mg concentrations due to basalt dissolution ($\Delta c_{Mg,basalt}$) and Mg-clay precipitation ($\Delta c_{Mg,clay}$) such that

$$c_{Mg,measured} = X_{fw}\, c_{Mg,fw} + X_{inject}\, c_{Mg,inject} + \Delta c_{Mg,basalt} - \Delta c_{Mg,clay} \quad (1)$$

where X_{fw} and X_{inject} are the fraction of formation water and injected water in the collected monitoring well sample, determined by the concentrations of SF_6 and SF_5CF_3 tracers in these fluids (Matter et al., 2016) such that $X_{fw} + X_{inject} = 1$. If it can be assumed that the fluids mix and basalt dissolved prior to the precipitation of the Mg-bearing clay, the isotopic composition of the fluid before clay precipitation ($\delta^{26}Mg_1$) is given by

$$\delta^{26}Mg_1 = \frac{(\delta^{26}Mg_{fw}\, X_{fw}\, c_{Mg,fw} + \delta^{26}Mg_{inject}\, X_{inject}\, c_{Mg,inject} + \delta^{26}Mg_{basalt} \Delta c_{Mg,basalt})}{(X_{fw}\, c_{Mg,fw} + X_{inject}\, c_{Mg,inject} + \Delta c_{Mg,basalt})} \quad (2)$$

[1] The term conservative dissolution in this regard refers to a process where the dissolution releases to the fluid Mg having the same isotopic composition as the dissolving rock.

where $\delta^{26}Mg_i$ designates the isotopic composition of the indicated source. The Mg isotope compositions of the monitoring well samples can then be determined from an expression of the Rayleigh equation of the form:

$$\delta^{26}\mathrm{Mg}_{sampled\ fluid} = \delta^{26}\mathrm{Mg}_1 - f^{\Delta^{26}Mg_{clay-fluid}} \quad (3)$$

where $\delta^{26}\mathrm{Mg}_{sampled\ fluid}$ designates the isotopic composition in the sampled monitoring well fluid, $\Delta^{26}Mg_{clay-fluid}$ stands for the indicated isotope fractionation factor, and *f*, the fraction of the Mg remaining in the fluid following clay mineral precipitation in each sample. Equations (1) to (3) were solved simultaneously to generate the values of *f* shown in Fig. 4. The values of X_{fw} and X_{inject} in Eqn. (2) required for this calculations were taken from Matter et al. (2016), and values of $\delta^{26}\mathrm{Mg}_{inject}$ and $c_{\mathrm{Mg},inject}$ are provided in Tables 1 and 2. Note the $\delta^{26}\mathrm{Mg}_{fw}\ X_{fw}\ c_{\mathrm{Mg},fw}$ term is negligible compare to the other terms in Eqn. (2) due to the low Mg concentration of the pre-injection formation waters (compare the composition of sample 12KMG01 with the others in Table 2). The calculated fraction of the Mg remaining in solution into clay minerals, as shown in Fig. 4, tends to decrease with time. Calculations suggest that this fraction decreases continuously from 33 to 12 percent with time from February 8, 2012 to June 8, 2014. This behavior contrasts somewhat with the saturation index of Mg clays, which becomes undersaturated in the sampled monitoring fluids when the injected acid fluid first arrive at the monitoring well – see Table 2. It can be seen in Fig. 4 that the distribution of calculated Mg precipitation fractions exhibit a concave distribution consistent with the slowing of clay formation rates with time. Consistent with the very dilute Mg concentrations of the deep well fluid prior to the injection, it seems likely that this fraction would approach zero over the long-term.

This estimate, however, is likely a minimum estimate as evidence indicates that calcite dissolved into the gas charged injection waters shortly after they arrive in the subsurface (Matter et al., 2016; Snæbjörnsdóttir et al., 2017, 2018). The dissolution of these calcites would likely release some light Mg to the fluid phase. In addition, the dissolution of basaltic glass and olivine has been reported to initially release light Mg to

433 the fluid (Wimpenny et al., 2010). Indeed, mass balance and reactive path calculations
434 reported by Snæbjörnsdóttir et al. (2017, 2018) suggest that more than 95% of the Mg
435 release by dissolving basaltic glass needed to be incorporated into secondary phases to be
436 consistent with the measured dissolved Mg concentration of the HN-04 monitoring well
437 fluids in March 2013. The stable Mg isotope measurements reported here suggest that the
438 bulk of these secondary Mg phases formed following the CarbFix injections were Mg
439 bearing clays (e.g. smectite).
440
441 It should be emphasized, however, that the calculated results shown in Fig. 4 are
442 highly uncertain due to poor understanding of the Mg isotope fractionation factor
443 between Mg clay minerals and the aqueous fluid. For example, Teng et al. (2010)
444 suggested that the $\Delta^{26}Mg_{clay-fluid}$ deduced from the compositions of South Carolina
445 saprolites range from 0.05‰ to -0.4‰. In contrast, Huang et al. (2012) reported that
446 $\Delta^{26}Mg_{clay-fluid}$ based on the compositions of southern Chinese saprolites ranged from -
447 0.94‰ to -1.94‰. Wimpenny et al. (2014), however, concluded that the Huang et al.
448 (2012) observations were more consistent with a $\Delta^{26}Mg_{clay-fluid}$ of -0.57‰. The
449 computed value of *f*, the fraction of the Mg remaining in the fluid following clay mineral
450 precipitation in each sample determined in this study depends strongly on the value
451 chosen for $\Delta^{26}Mg_{clay-fluid}$. A value of $\Delta^{26}Mg_{clay-fluid}$ = -0.40‰ would yield a final f
452 value for the June 8, 2014 sample of 0.07, whereas a $\Delta^{26}Mg_{clay-fluid}$ = -1.00‰ would
453 yield a final f value for the June 8, 2014 sample of 0.34. Moreover, it should also be
454 noted that at the pH and fluid composition changed (Schott et al., 2016), so too would
455 $\Delta^{26}Mg_{clay-fluid}$. Such changes also would alter the calculated values of *f*. It follows
456 that precise and accurate values of $\Delta^{26}Mg_{clay-fluid}$ are an essential prerequisite to using
457 the compositions the Mg isotopic compositions of minerals and fluids to quantify natural
458 geochemical processes.
459
460 The formation of Mg clays in response to the injection of CO_2 into basalts, as
461 indicated in this study, is detrimental to carbon storage efforts for two main reasons.
462 First, the formation of these Mg-bearing silicates consume divalent Mg that could

otherwise be used for the formation of carbonate minerals. Second, Mg-bearing clays are voluminous, such that they consume valuable porosity and could decrease host rock permeability. The formation of these clays, however, will occur at a distance from the injection well, as their precipitation requires sufficient basalt dissolution to increase the fluid pH to at least 7 (Snæbjörnsdóttir et al., 2017). As such their formation will not likely clog flow pathways near the injection well. Nevertheless, their formation at a distance from these wells will limit somewhat the efficiency of carbon storage efforts in basalts. This potential challenge might be overcome by injecting at higher temperatures, where the formation of magnesite rather than Mg-bearing clays might be favored, however, Mg-silicate alteration phases including mixed-layered clays, chlorite, and epidote are common alteration phases in basalts to at least 280 ^{o}C (Snæbjörnsdóttir et al., 2018). Nevertheless, the continuous injection of acidic CO_2-charged fluids may lead to a propagating reaction front that would progressively move these clay minerals further away from the injection well.

6. Conclusions

The Mg isotope compositions of monitoring well samples collected in this study are lighter than the host basalts that dissolved in response to the injection of gas charged waters into the CarbFix site. This observation is consistent with the consumption of the divalent Mg cations released by basalt dissolution by isotopically heavier Mg clay minerals, rather than carbonate minerals, which tend to favor the incorporation of isotopically light Mg. This conclusion is supported by the fact that Mg-smectites rather than Mg carbonate phases are commonly observed as secondary phases in basalts altered at low temperatures. Such results demonstrate that the Mg isotopic compositions of monitoring well fluids can be used to provide insight into the fate of Mg during subsurface carbon storage efforts.

The rates at which Mg precipitates as clay minerals appear to be relatively slow; mass balance calculations suggest that smectite is still continuing to precipitate 2 years after the termination of the acid gas injection – calculations suggest that ~12 percent of the Mg released to the fluid by basalt dissolution remains to be precipitated after two

494 years. This contrasts with calcite, which has demonstrated to precipitate more than 95%
495 of the injected CO_2 in less than 2 years (Matter et al., 2016). Although Mg clay mineral
496 precipitation is relatively slow, its precipitation may limit significantly the efficiency of
497 carbon storage efforts based on the enhanced weathering of mafic or ultramafic rocks
498 over the long term (Rigopoulos et al., 2018).
499
500 *Acknowledgements*- We acknowledge funding from the Environmental Fund of
501 Reykjavik Energy, the European Commission through the projects CarbFix (EC
502 coordinated action 283148), CarbFix2 (Grant Agreement No, 764760), Min-GRO (MC-
503 RTN-35488), Delta-Min (PITN-GA-2008-215360), and CO_2-REACT (EC Project
504 317235), the U.S. Department of Energy under award number DE-FE0004847, the
505 Nordic fund 11029-NORDICCS, and the Icelandic GEORG Geothermal Research fund
506 (09-02-001). We are indebted to Hólmfríður Sigurðardóttir at Reykjavík Energy, Magnús
507 Þór Arnarson at Mannvit Engineering, Domenik Wolff-Boenisch at Curtin University in
508 Australia, Helgi A. Alfreðsson at the University of Iceland and Wallace S. Broecker at
509 Columbia University for their contributions to the CarbFix project. We thank Einar Örn
510 Þrastarson, Trausti Kristinsson, Vordís Eiríksdóttir, Halldór Bergmann, and Þorsteinn A.
511 Þorgeirsson at Reykjavík Energy; Vigdís Harðardóttir, Finnbogi Óskarsson, Kristján
512 Hrafn Sigurðsson and Steinþór Níelsson at ISOR; Jennifer Hall at Columbia University,
513 Franziska Stamm at GET Toulouse, and Þorsteinn Jónsson, Sveinbjörn Steinþórsson,
514 Iwona Galezcka, Eydís S. Eiríksdóttir, Deirdre Clark, Chris Grimm and Flora Brocza at
515 the University of Iceland for helping the injection and sampling campaign.
516

517 ## 7. References

518 Alfredsson, H. A., Oelkers, E. H., Hardarsson, B. S., Franzson, H., Gunnlaugsson, E., and
519 Gislason, S.R. (2013) The geology and water chemistry of the Hellisheidi, SW-Iceland carbon
520 storage site. *Int. J. Greenhouse Gas Cont.* **12,** 399-418.

521 Alfredsson, H. A., Mesfin, K.G., and Wolff-Boenisch, D. (2016) The syringe sampler: An
522 inexpensive alternative borehole sampling technique for CO_2-rich fluids during mineral carbon
523 storage. *Greenhouse Gases: Sci. Tech.* **6,** 167-177.

524 An, Y.J., and Huang, F. (2014) A review of Mg isotope analytical methods by MC-ICP-MS. *J.*
525 *Earth Sci.-China* **25,** 822-840.

526 Aradóttir, E., Sigurdardóttir, H., Sigfússon, B., and Gunnlaugsson, E. (2011). CarbFix: A CCS
527 pilot project imitating and accelerating natural CO_2 sequestration. *Greenhouse Gas Sci*
528 *Technol,* **1,** 105-118.

529 Aradóttir, E., and Hjalmarsson, E. (2018) CarbFix – Public engagement and transparency. *Energy*
530 *Procedia,* **146,** 115-120

531 Archer, D. (2005) Fate of fossil fuel CO_2 in geologic time. *J. Geophys. Res.* **110,** C09S05.

532 Assayag, N., Matter, J., Ader, M., Goldberg, D., and Agrinier, P., 2009. Water–rock interactions
533 during a CO_2 injection field-test: Implications on host rock dissolution and alteration effects.
534 *Chem. Geol.* **265,** 227-235.

Bacon, D. H., Ramanathan, R., Schaef, H. T., and McGrail, B. P. (2014) Simulating geologic co-sequestration of carbon dioxide and hydrogen sulfide in a basalt formation. *Int. J. Greenhouse Gas Control* **21,** 165-176.

Beinlich, A., Mavromatis, V., Austrheim, H., and Oelkers E.H. (2012) Inter-mineral Mg isotope fractionation during hydrothermal ultramafic rock alteration – Implications for the global Mg-cycle. *Earth Planet. Sci. Let.* **392,** 166-76.

Black, J.R., Yin, Q.Z., Casey, W.H. (2006) An experimental study of magnesium-isotope fractionation in chlorophyll-a photosynthesis. *Geochim. Cosmochim. Acta* **70,** 4072-4079.

Bolou-Bi, E.B., Vigier, N., Brenot, A. and Poszwa, A. (2009) Magnesium isotope compositions of natural reference materials. *Geostand. Geoanal. Res.* **33**, 95-109.

Bolou-Bi, E.B., Poszwa, A., Leyval, C., Vigier, N. (2010) Experimental determination of magnesium isotope fractionation during higher plant growth. *Geochim. Cosmochim. Acta* **74**, 2523-2537.

Bolou-Bi, E.B., Vigier, N., Poszwa, A., Boudot, J.-P., Dambrine, E. (2012) Effects of biogeochemical processes on magnesium isotope variations in a forested catchment in the Vosges Mountains (France). *Geochim. Cosmochim. Acta* **87,** 341–355.

Brenot, A., Cloquet, C., Vigier, N., Carignan, J., and France-Lanord, C. (2008) Magnesium isotope systematics of the lithologically varied Moselle river basin, France. *Geochim. Cosmochim. Acta* **72,** 5070-5089.

Buhl, D., Immenhauser, A., Smeulders, G., Kabiri, L. and Richter, D.K. (2007) Time series δ^{26}Mg analysis in speleothem calcite: Kinetic versus equilibrium fractionation, comparison with other proxies and implications for palaeoclimate research. *Chem. Geol.* **244,** 715-729.

Chang, V.T.C., Williams, R.J.P., Makishima, A., Belshawl, N.S. and O'Nions, R.K. (2004) Mg and Ca isotope fractionation during $CaCO_3$ biomineralisation. *Biochem. Biophys. Res. Comm.* **323,** 79-85.

Croviser, J.L., Honnorez, J., Britz, B., and Petit, J.-C. (1992) Dissolution of subglacial volcanic glasses from Iceland: Laboratory study and modelling. *Appl. Geochem.,* **7**, Supplement 1, 55-81.

Fisher, A. T. (1998) Permeability within basaltic oceanic crust: *Revs. Geophys.* **36,** 143-182.

Flaathen, T. K., Gislason, S. R., Oelkers, E. H., and Sveinbjörnsdóttir, Á. E. (2009) Chemical evolution of the Mt. Hekla, Iceland, groundwaters: A natural analogue for CO_2 sequestration in basaltic rocks. *App. Geochem.* **24,** 463-474.

Foster, G.L., Pogge von Strandmann, P.A.E., and Rae, J.W.B. (2010) The boron and magnesium isotopic composition of seawater. *Geochemistry Geophysics Geosystems* **11**, Q08015, doi:10.1029/2010GC003201.

Galeczka, I., Wolff-Boenisch, D., Oelkers, E. H., and Gislason, S. R. (2014) An experimental study of basaltic glass–H_2O–CO_2 interaction at 22 and 50°C: Implications for subsurface storage of CO_2. *Geochim. Cosmochim. Acta* **126,** 123-145.

Galy, A., Bar-Matthews, M., Halicz, L and O'Nions, R. K. (2002) Mg isotopis compostion of carbonate: In sight from speleothem formation. *Earth. Planet. Sci. Let.* **202,** 105-115.

Galy, A., Yoffe, O., Janney, P.E., Williams, R.E., Cloquet, C., Alard, O., Halicz, L., Wadwha, A., Hutchen, I.D., Ramon, E. and Carignan, J. (2003) Magnesium isotopes heterogeneity of the isotopic standard SRM980 and new reference materials for magnesium-isotope-ratio measurements. *J. Anal. At. Spectrom.* **18,** 1352-1356.

579 Geske, A., Goldstein, R.H., Mavromatis, V, Richter, D.K., Buhl, D., Kluge, T., John, C.M., and
580 Immenhauser, A. (2015) The magnesium isotope (δ^{26}Mg) signature of dolomites. *Geochim.*
581 *Cosmochim. Acta* **149,** 131–151.

582 Geske, A., Zorlu, J., Richter, D.K., Buhl, D., Niedermayr, A., and Immenhauser, A. (2012)
583 Impact of diagenesis and low grade metamorphosis on isotope (δ^{26}Mg, δ^{13}C, δ^{18}O and
584 ^{87}Sr/^{86}Sr) and elemental (Ca, Mg, Mn, Fe and Sr) signatures of Triassic sabkha dolomites.
585 *Chem. Geol.* **332–333,** 45–64.

586 Gíslason, S. R., Arnorsson, S. and Armannsson, H. (1996) Chemical Weathering of Basalt in
587 Southwest Iceland; Effects of Runoff, Age of Rocks and Vegetative/glacial Cover. *Am. J.*
588 *Sci*. **296,** 837-907.

589 Gíslason, S. R., Broecker, W. S., Gunnlaugsson, E., Snæbjörnsdóttir, S. Ó., Mesfin, K. G.,
590 Alfredsson, H. A., Aradottir, E. S., Sigfusson, B., Gunnarsson, I., Stute, M., Matter, J. M.,
591 Arnarson, M. T., Galeczka, I. M., Guðbrandsson, S., Stockman, G., Wolff-Boenisch, D.,
592 Stefansson, A., Ragnheidardottir, E., Faathen, T., Gysi, A. P., Olssen, J., Didriksen, K., Stipp,
593 S., Menez, B., and Oelkers, E. H. (2014) Rapid solubility and mineral storage of CO_2 in basalt.
594 *Energy Procedia* **63**, 4561-4574.

595 Gíslason, S.R. and Oelkers, E.H. (2003) Mechanism, rates, and consequences of basaltic glass
596 dissolution: II. An experimental study of the dissolution rates of basaltic glass as a function of
597 pH and temperature. *Geochim. Cosmochim. Acta* **67,** 3817-3832.

598 Gíslason, S. R., and Oelkers, E. H. (2014) Carbon Storage in Basalt. *Science,* **344,** 373-374.

599 Gíslason, S. R., Wolff-Boenisch, D., Stefansson, A., Oelkers, E. H., Gunnlaugsson, E.,
600 Sigurdardottir, H., Sigfusson, B., Broecker, W.S., Matter, J. W., and Stute. M. (2010) Mineral
601 Sequestration of Carbon Dioxide in Basalt: A Pre-injection Overview of the CarbFix
602 project. *Int. J. Greenhouse Gas Cont*. **4,** 537-45.

603 Gíslason, S. R., Sigurdardóttir, H., Aradóttir, E. S., and Oelkers, E.H. (2018) A brief history of
604 CarbFix: challenges and victories of the project's phase. *Energy Procedia,* **146,** 103-114.

605 Goldberg, D. and Slagle, A.L. (2009) A global assessment of deep-sea basalt sites for carbon
606 sequestration. En*ergy Procedia* **1**, 3675-3682.

607 Goldberg, D., Lackner, K., Han, P., and Wang, T. (2013) Co-Location of Air Capture,
608 Subseafloor CO_2 Sequestration, and Energy Production on the Kerguelen Plateau: *Envir. Sci.*
609 *Tech.* **47**, 7521-7529.

610 Goldberg, D. S., Takahashi, T., and Slagle, A. L. (2008) Carbon dioxdie sequestration in deep-sea
611 basalt. *PNAS* **105,** 9920-9925.

612 Goldberg, D. S., Kent, D. V., and Olsen, P. E. (2010) Potential on-shore and off-shore reservoirs
613 for CO_2 sequestration in Central Atlantic magmatic province basalts. *PNAS,* **107,** 1327-1332.

614 Gudbrandsson, S., Wolff-Boenisch, D., Gislason, S. R., and Oelkers, E. H. (2011) An
615 experimental study of crystalline basalt dissolution from $2 < pH < 11$ and temperatures from 5
616 to 75 °C. *Geochim. Cosmochim. Acta* **75,** 5496-5509.

617 Gysi, A. P., and Stefánsson, A. (2012) CO_2-water–basalt interaction. Low temperature
618 experiments and implications for CO_2 sequestration into basalts: *Geochim. Cosmochim. Acta*
619 **81,**129-152.

620 Harris, R. N., and Chapman, D. S. (2004) Deep-seated oceanic heat flux, heat deficits and
621 hydrothermal circulation, Cambridge, Cambridge University Press, Hydrogeology of the
622 Oceanic Lithosphere.

623 Higgins, J.A. and Schrag, D.P. (2010) Constraining magnesium cycling in marine sediments
624 using magnesium isotopes. *Geochim. Cosmochim. Acta* **74**, 5039-5053.

625 Hin, R.C., Coath, C.D., Carter, P.J., Nimmo, F., Lai, Y.-L., Pogge von Strandmann, P.A.E.,
626 Willbold, M., Leinhardt, Z.M., Walter, M.J., Elliott, T., (2017) Magnesium isotope evidence
627 that accretional vapour loss shapes planetary compositions. *Nature* **549,** 511-515.

628 Hippler, D., Buhl, D., Witbaars, R.m, Richter, D.K., and Immenhauser, A. (2009) Towards a
629 better understanding of magnesium-isotope rations from marine skeletons. *Geochim.*
630 *Cosmochim. Acta* **73**, 6134-6146.

631 Huang K.-J., Teng F.-Z., Wei G.-J., Ma J.-L., and Bao Z.-Y. (2012) Adsorption- and desorption-
632 controlled magnesium isotope fractionation during extreme weathering of basalt in Hainan
633 Island, China. *Earth Planet. Sci. Let.* **359–360,** 73–83.

634 Immenhauser, A., Buhl, D., Richter, D., Niedermayr, A., Riechelmann, D., Dietzel, M., and
635 Schulte, U. (2010) Magnesium-isotope fractionation during low-Mg calcite precipitation in a
636 limestone cave - Field study and experiments. *Geochim. Cosmochim. Acta* **74,** 4346-4364.

637 Khalilabad, M.R., Axelsson, G. and Gislason, S.R. (2008) Aquifer characterization with tracer
638 test technique; permanent CO_2 sequestration into basalt, SW Iceland. *Min. Mag.* **72,** 121-125.

639 Li, W., Chakraborty, S., Beard, B.L., Romanek, C.S., and Johnson, C.M. (2012) Magnesium
640 isotope fractionation during precipitation of inorganic calcite under laboratory conditions.
641 *Earth and Planet. Sci. Let.* **333-334,** 304-316.

642 Li, W., Beard, B.L., Li, C., Xu, H., and Johnson, C.M. (2015) Experimental calibration of Mg
643 isotope fractionation between dolomite and aqueous solution and its geological implications.
644 *Geochim. Cosmochim. Acta* **157,** 164-181.

645 Li, W., Beard, B.L., Li, C., and Johnson, C.M. (2014) Magnesium isotope fractionation between
646 brucite [$Mg(OH)_2$] and Mg aqueous species: Implications for silicate weathering and
647 biogeochemical processes. *Earth and Planet. Sci. Let.* **394,** 82-93.

648 Ling, M.X., Sedaghatpour, F., Teng, F.-Z., Hays, P.D., Strauss, J., Sun, W.D. (2011)
649 Homogeneous magnesium isotopic composition of seawater: an excellent geostandard for Mg
650 isotope analysis. *Rapid. Commun. Mass Sp.* **25**, 2828-2836

651 Liu, P.-P., Teng, F.-Z., Dick, H. J. B., Zhou, M.-F., and Chung S.-L. (2017) Magnesium isotopic
652 composition of the oceanic mantle and oceanic Mg cycling. *Geochim. Cosmochim. Acta* **206,**
653 151-165.

654 Liu, X-M., F-Z. Teng,F.-Z,. Rudnick, R. L., Mcdonough, W. F. and Cummings, M. L. (2014)
655 Massive magnesium depletion and isotope fractionation in weathered basalts. *Geochim.*
656 *Cosmochim. Acta* **135,** 336-349.

657 Maher, K., Johnson, N.C., Jackson, A., Lammers, L.N., Torchinsky, A.B., Weaver, K.L., Bird,
658 D.K., Brown, G.E. (2016) A spatially resolved surface kinetic model for forsterite dissolution.
659 *Geochim. Cosmochim. Acta* **174**, 313-334.

660 Marieni, C., Prikryl, J., Aradottir, E.S., Gunnarsson, I., and Stefansson, A. (2018) Towards
661 'green' geothermal energy: Co-mineralization of carbon and sulphur in geothermal reservoirs.
662 *Int. J. Greenhouse Gas Cont.,* **77,** 96-105.
663 Matter, J. M., Broecker, W., Stute, M., Gislason, S., Oelkers, E., Stefánsson, A., Björnsson, G.
664 (2009) Permanent carbon dioxide storage into basalt: The CarbFix pilot project,
665 Iceland. *Energy Procedia,* **1,** 3641-3646.

Matter, J., Takahashi, T., and Goldberg, D. (2007) Experimental evaluation of *in situ* CO_2-water-rock reactions during CO_2 injection in basaltic rocks: Implications for geological CO_2 sequestration: *Geochem. Geophy. Geosy.* **6,** 19.

Matter, J.M., Stute, M., Snæbjörnsdóttir, S.Ó., Oelkers, E.H., Gislason, S.R., Aradottir, E.S., Sigfusson, B., Gunnarsson, I., Sigurdardottir, H., Gunnlaugsson, E., Axelsson, G., Alfredsson, H.A., Wolff-Boenisch, D., Mesfin, K., Fernandez de la Reguera Taya, D., Hall, J., Dideriksen, K. and Broecker, W.S. (2016) Rapid carbon mineralization for permanent and safe disposal of anthropogenic carbon dioxide emissions. *Science* **352,** 1312-1314.

Mavromatis, V., Gautier, Q., Bosc, O. and Schott, J. (2013) Kinetics of Mg partition and Mg stable isotope fractionation during its incorporation in calcite. *Geochim. Cosmochim. Acta* **114**, 188-203.

Mavromatis, V., Meister, P. and Oelkers, E.H. (2014) Using stable Mg isotopes to distinguish dolomite formation mechanisms: A case study from the Peru Margin. *Chem. Geol.* **385**, 84-91.

Mavromatis, V., Pearce, C.R., Shirokova, L.S., Bundeleva, I.A., Pokrovsky, O.S., Benezeth, P. and Oelkers, E.H. (2012) Magnesium isotope fractionation during hydrous magnesium carbonate precipitation with and without cyanobacteria. *Geochim. Cosmochim. Acta* **76**, 161-174.

McGrail, B. P., Freeman, C. J., Brown, C. F., Sullivan, E. C., White, S. K., Reddy, S., Garber, R. D., Tobin, D., Gilmartin, J. J., and Steffensen, E. J. (2012) Overcoming business model uncertainty in a carbon dioxide capture and sequestration project: Case study at the Boise White Paper Mill. *Int. J. Greenhouse Gas Cont.* **9**, 91-102.

McGrail, B. P., Schaef, H. T., Ho, A. M., Chien, Y.-J., Dooley, J. J., and Davidson, C. L. (2006) Potential for carbon dioxide sequestration in flood basalts. *J. Geophys, Res. Solid Earth* **111,** B12201.

McGrail, B. P., Spane, F. A., Sullivan, E. C., Bacon, D. H., and Hund, G. (2011) The Wallula basalt sequestration pilot project. *Energy Procedia* **4,** 5653-5660.

Norman, M.D., Yaxley, G.M., Bennett, V.C., and Brandon, A.D. (2006) Magnesium isotopic composition of oliving from ther Earth, Mars, Moon and pallasite parent body. *Geophys. Res. Let.,* **33,** L15202.

Oelkers, E. H. (2001) General kinetic description of multioxide silicate mineral and glass dissolution. *Geochim. Cosmochim. Acta* **65,** 3703-3719.

Oelkers, E.H. and Gislason, S.R. (2001) The mechanism, rates and consequences of basaltic glass dissolution: I. An experimental study of the dissolution rates of basaltic glass as a function of aqueous Al, Si and oxalic acid concentration at 25°C and pH = 3 and 11. *Geochim. Cosmochim. Acta* **65**, 3671-3681.

Oelkers, E. H., Gislason, S. R., and Matter, J. M. (2008) Mineral carbonation of CO_2. *Elements,* **4,** 333-337.

Oelkers, E.H., Benning, L.G., Lutz, S., Mavromatis, V., Pearce, C.R. and Plümper, O. (2015) The efficient long-term inhibition of forsterite dissolution by common soil bacteria and fungi at Earth surface conditions. *Geochim. Cosmochim. Acta* **168**, 222-235.

Opfergelt, S., Geors, R.B., Burton. K.W., Guicharnaud, R., Siebert, C., Gislason, S. R., and Halliday, A.N. (2011) Seasonal magnesium isotope variations in soil solutions reflecting physico-chemical processes controlling soil weathering fluxes. *Min. Mag.* **75**, 1571.

709 Opfergelt, S., Burton, K., Georg, R., West, A., Guicharnaud, R., Sigfusson, B., Seibert, C.,
710 Gislason, S.R. and Halliday, A. (2014) Magnesium retention on the soil exchange complex
711 controlling Mg isotope variations in soils, soil solutions and vegetation in volcanic soils,
712 Iceland. *Geochim. Cosmochim. Acta* **125,** 110-130.

713 Olsson, J., Stipp, S. L. S., Makovicky, E., and Gislason, S. R. (2014) Metal scavenging by
714 calcium carbonate at the Eyjafjallajökull volcano: A carbon capture and storage analogue.
715 *Chem. Geol.* **384,** 135-148.

716 Pearce, C. R., Saldi, G. D., Schott, J., and Oelkers, E. H. (2012) Isotopic fractionation during
717 congruent dissolution, precipitation and at equilibrium: Evidence from Mg isotopes. *Geochim.*
718 *Cosmochim. Acta* **92,** 170-183.

719 Pogge von Strandmann, P.A.E., Burton, K.W., James, R.H., van Calsteren, P., Gislason, S.R. and
720 Sigfusson, B. (2008) The influence of weathering processes on riverine magnesium isotopes in
721 a basaltic terrain. *Earth Planet Sci. Let.* **276**, 187-197.

722 Pogge von Strandmann, P.A.E., Opfergelt, S., Lai, Y.-J., Sugfusson, B., Gislason. S.R. and
723 Burton, K.W. (2011) Variations of Li and Mg isotope ratios in bulk chondrites and mantle
724 xenoliths. *Geochim. Cosmochim. Acta* **75,** 5247–5268.

725 Pogge von Strandmann, P.A.E., Elliott, T., Marschall, H. R., Coath, C., Lai, Y.-J., Jeffcoate, A.
726 B., and Ioanoc, D. A. (2012) Lithium, magnesium and silicon isotope behaviour
727 accompanying weathering in a basaltic soil and pore water profile in Iceland. *Earth Planet.*
728 *Sci. Let.* **339–340,** 11–23.

729 Pogge von Strandmann, P. A. E., Forshaw, J., and Schmidt, D. (2014) Modern and Cenozoic
730 records of seawater magnesium from foraminiferal Mg isotopes. *Biogeosciences,* 5155-5168.

731 Pokharel, R., Gerrits, R., Schuessler, J.A., Floor, G., Gorbushina, A.A., and von Blanckenburg, F.
732 (2017) Mg isotope fractionation during uptake by a rock-inhabiting, model microcolonial
733 fungus Knufia petricola at acidic and neutral pH. *Environ. Sci. Tech.* **51**, 9691-9699.

734 Prikryl, J., Stefansson, A., and Pearce, C.R. (2018) Tracing olivine carbonation and
735 serpentinization in CO_2-rich fluids via magnesium exchange and isotopic fractionation.
736 *Geochim. Cosmochim. Acta* **243,** 133-148.

737 Rigopoulos, I., Harrison, A.L., Delimitis, A., Ioannou, I., Efastathiou, A.M., Kyratsi, T., and
738 Oelkers, E.H. (2018) Carbon sequestration via enhanced weathering of peridotes and basalts in
739 seawater. *App. Geochem.* **91,** 197-218.

740 Rogers, K. L., Neuhoff, P. S., Pedersen, A. K., and Bird, D. K. (2006) CO_2 metasomatism in a
741 basalt-hosted petroleum reservoir, Nuussuaq, West Greenland. *Lithos,* **92**, 55-82.

742 Rosenbauer, R. J., Thomas, B., Bischoff, J. L., and Palandri, J. (2012) Carbon sequestration via
743 reaction with basaltic rocks: Geochemical modelling and experimental results. *Geochim.*
744 *Cosmochim. Acta* **89**, 116−133.

745 Ryu, J-S., Vigier, N., Decarreau, A., Lee, S.-W., Lee, K.-S., Song, H., and Petit, S. (2016)
746 Experimental investigation of Mg isotope fractionation during mineral dissolution and clay
747 formation. *Chem. Geol.* **445,** 135-145.

748 Saenger, C., and Wang, Z. (2014) Magnesium isotope fractionation in biogenic and abiogenic
749 carbonates: Implications for paleoenvironmental proxies. *Quaternary Sci. Revs.* **90,** 1-21.

750 Saulnier, S., Rollion-Bard, C., Vigier, N. and Chaussidon, M. (2012) Mg isotope fractionation
751 during calcite precipitation: An experimental study. *Geochim. Cosmochim. Acta* **91,** 75-91.

752 Schott, J., Mavromatis, V., Fujii, T., Pearce, C.R., and Oelkers, E.H. (2016) The control of
753 carbonate mineral Mg isotope composition by aqueous speciation: Theoretical and
754 experimental modeling. *Chem. Geol.* **445,** 120–134.

755 Shirokova, L. S., Mavromatis, V., Bundeleva, I.A., Pokrovsky, O.S., Bénézeth, P., Gérard, E.,
756 Pearce, C. R., and Oelkers, E.H. (2012) Using Mg Isotopes to trace cyanobacterially mediated
757 magnesium carbonate precipitation in alkaline lakes. *Aquat. Geochem.* **19,** 1-24.

758 Sigfusson, B., Gislason, S. R., Matter, J. M., Stute, M., Gunnlaugsson, E., Gunnarsson, I.,
759 Aradottir, E. S., Sigurdardottir, H., Mesfin, K. G., Alfredsson, H. A., Wolff-Boenisch, D.,
760 Arnarson, M. T., and Oelkers, E. H. (2015) Solving the carbon-dioxide buoyancy challenge:
761 The design and field testing of a dissolved CO_2 injection system. *Int. J. Greenhouse Gas Cont.*
762 **37,** 213-219.

763 Sigfusson, B., Arnarson, M. T., Snæbjörnsdóttir, S.Ó., Karlsdóttir, M. R., Aradottir, E. S., and
764 Gunnarsson, I. (2018) Reducing emissions of carbon dioxide and hydrogen sulphide at
765 Hellishidi power plant in 2014-2017 and the role of CarbFix in achieving the 2040 Iceland
766 climate goals. *Energy Procedia* **146**, 135-145.

767 Snæbjörnsdóttir, S.Ó., Wiese, F., Fridriksson, T., Ármannsson, H., Einarsson, G.M. and Gislason,
768 S.R. (2014) CO_2 storage potential of basaltic rocks in Iceland and the oceanic ridges. *Energy*
769 *Procedia* **63**, 4585-4600.

770 Snæbjörnsdóttir, S.Ó., Oelkers, E.H., Mesfin, K., Aradóttir, E.S., Dideriksen, K., Gunnarsson, I.,
771 Gunnlaugsson, E., Matter, J.M., Stute, M. and Gislason, S.R. (2017) The chemistry and
772 saturation states of subsurface fluids during the in situ mineralisation of CO_2 and H_2S at the
773 CarbFix site in SW-Iceland. *Int. J. Greenhouse Gas Cont.* **58,** 87-102.

774 Snæbjörnsdóttir, S.Ó., Gislason, S.R., Galecka, I.M., and Oelkers, E.H. (2018) Reaction path
775 modelling of in-situ mineralisation of CO_2 at the CarbFix site at Hellishedi, SW-Iceland. .
776 *Geochim. Cosmochim. Acta.* **58,** 87-102.

777 Snæbjörnsdóttir, S.Ó., Tomasdottir, S., Sigfusson, B., Aradóttir, E.S., Gunnarsson, G., Niemi, A.,
778 Basirat, F., Gislason, S.R., Oelkers, E.H., and Franzson, H. (2018) The geology and hydrology
779 ofghe CarbFix2 site, SW-Iceland. *Energy Procedia* **146**, 146-157.

780 Stefánsson, A., Arnórsson, S., Gunnarsson, I., Kaasalainen, H., and Gunnlaugsson, E., 2011. The
781 geochemistry and sequestration of H_2S into the geothermal system at Hellisheidi, Iceland. *J.*
782 *Volcan. Geothermal Res.* **202,** 179-188.

783 Stockmann, G. J., Wolff-Boenisch, D., Gislason, S. R., and Oelkers, E. H. (2011) Do carbonate
784 precipitates affect dissolution kinetics? 1: Basaltic glass. *Chem. Geol.* **284,** 306-316.

785 Teng, F.-Z., Wadhwa, M., and Helz, R. T. (2007) Investigation of magnesium isotope
786 fractionation during basalt differentiation: Implications for a chondritic composition of the
787 terrestrial mantle. *Earth Planet. Sci. Let.* **261**, 84-92.

788 Teng, F.-Z., Li, W., Rudnick, R. L., and Gardner, L. R. (2010a) Contrasting lithium and
789 magnesium isotope fractionation during continental weathering. *Earth Planet. Sci. Let.* **300,**
790 63-71.

791 Teng, F.-Z. (2017) Magnesium Isotope Geochemistry. *Revs. Min. Geochem.* **82,** 219-287.

792 Tipper, E., A. Galy, A., Gaillardet, J. Bickle, M., Elderfield H., and Carder, E. (2006a) The
793 magnesium isotope budget of the modern ocean: Constraints from riverine magnesium isotope
794 ratios. *Earth Planet. Sci. Let.* **250**, 241-253.

795 Tipper, E.T., Galy, A. and Bickle, M.J. (2006b) Riverine evidence for a fractionated reservoir of
796 Ca and Mg on the continents: Implications for the oceanic Ca cycle. *Earth Planet. Sci. Let.*
797 **247,** 267-279.

798 Tipper, E.T., Galy, A., and Bickle, M. (2008) Calcium and magnesium isotope systematics in
799 rivers draining the Himalaya-Tibetan-Plateau region: Lithological or fractionation control?
800 *Geochim. Cosmochim. Acta* **72,** 1057-1075.

801 Tipper, E.T., Calmels, D., Gaillardet, J., Louvet, P., Capmas, F., and Dubacq, B. (2012a) Positive
802 correlation between Li and Mg isotope ratios in the river waters of the Mackenzie Basin
803 challenges the interpretation of apparent isotopic fractionation during weathering. *Earth*
804 *Planet. Sci. Let.* **333,** 35-45

805 Tipper, E.T., Lemarchand, E., Hindshaw, R.S., Reynolds, B.C. and Bourdon, B. (2012b) Seasonal
806 sensitivity of weathering processes: Hints from magnesium isotopes in a glacial stream. *Chem.*
807 *Geol.* **312–313,** 80–92.

808 Uhlig, D., Schuessler, J.A., Bouchez, J.L., Dixon, J., and von Blanckenburg, F. (2017)
809 Quantifying nutrient uptake as driver of rock weathering in forest ecosystems by magnesium
810 stable isotopes. *Biogeosciences* **14**, 3111-3128.

811 Van Pham, H., Aagaard, P., and Hellevang, H. (2012) On the potential for CO_2 mineral storage in
812 continental flood basalts - PHREEQC batch and 1D diffusion - reaction simulations:
813 *Geochem. Trans.* **13,** 12.

814 Wimpenny, J., Gíslason, S.R., James, R. H., Gannoun, A., Pogge Von Strandmann, P.A.E., and
815 Burton, K.W. (2010) The behaviour of Li and Mg Isotopes during primary phase dissolution
816 and secondary mineral formation in basalt. *Geochim. Cosmochim. Acta* **74,** 5259-279.

817 Wimpenny, J., Colla, C.A., Yin, Q.Z., Rustad, J.R., Casey, W.H. (2014) Investigating the
818 behaviour of Mg isotopes during the formation of clay minerals. *Geochim. Cosmochim. Acta*
819 **128,** 178–194.

820 Wolff-Boenisch, D., Wenau, S., Gislason, S. R., and Oelkers, E. H. (2011) Dissolution of basalts
821 and peridotite in seawater, in the presence of ligands, and CO_2: Implications for mineral
822 sequestration of carbon dioxide: G*eochim. Cosmochim. Acta* **75,** 5510-5525.

823 Wombacher, F., Eisenhauer, A., Bohm, F., Gussone, N., Regenberg, M., Dullo, W.-Chr., and
824 Ruggeberg, A. (2011) Magnesium stable isotope fractionation in marine biogenic calcite and
825 aragonite. *Geochim. Cosmochim Acta* **75,** 5797-5818.

826 Young, E. D., and Galy, A. (2004) The isotope geochemistry and cosmochemistry of magnesium.
827 *Revs Min. Geochem.* **55,** 197-230.
828

Figure Captions

Fig. 1. Maps showing location of the study area (a) Map showing active volcanic zones in Iceland: RP = Reykjanes Peninsula, WVZ = Western Volcanic Zone, SISZ = South Iceland Seismic Zone, MVZ = Mid-Iceland Volcanic Zone, EVZ = Eastern Volcanic Zone and NVZ = Northern Volcanic Zone. (b) Map showing location of central volcanoes (dark gray) on Reykjanes Peninsula and associated fissure swarms (gray). (c) Map of the CO_2 injection site in, Hellisheidi, SW-Iceland. The CarbFix wells are shown as labeled gray dots. Mapped bedrock faults are located toward east and are part of the Hengill fissure swarm - after Alfredsson et al. (2013).

Fig 2. The temporal evolution of a) pH and b) Mg concentration of fluids collected from the HN-04 monitoring well, located 500 m away from the HN-02 injection well before during and after the injection of gas charged waters at the CarbFix site. The timing of the two injections is indicated by the two blue bars. Data from Snæbjörnsdóttir et al. (2017) and Alfredsson et al. (2013). The reported uncertainties on these analyses were reported to be ±0.02 units on pH and ±3% on the Mg concentration analyses.

Fig 3. The temporal evolution of $\delta^{26}Mg$ of fluids collected from the CarbFix site. Open diamonds illustrate the compositions of shallow wells prior to the injection, whereas the filled circles represent the composition of monitoring well samples. The dashed horizontal line shows the compositions of the basalts at the CarbFix site whereas the timing of the two injections is indicated by the two blue bars – see text.

Fig 4. The temporal evolution of the fraction of Mg released by basalt dissolution that has been incorporated into clay minerals ($f_{Mg,\,clay}$). Fractions were calculated assuming a closed-system Rayleigh model (see text).

Table 1. Summary of measured Mg isotopic compositions of pre-injection shallow well fluids, and post-injection monitoring well fluids collected from HN-04. All isotopic compositions were measured at the HELGES lab, GFZ Potsdam. 2SD refers to twice the standard deviation of n MC-ICP-MS measurements of the same solution. The uncertainty of the presented data (relevant for geological interpretation) is estimated to be 0.10 ‰ (2SD) for δ^{26}Mg and 0.06 ‰ (2SD) for δ^{25}Mg based on long-term repeated analyses of samples and references materials – see text.

sample	date (day/month /year)	c_{Mg} (mol kg^{-1}) x 10^{-6}	$\delta^{25}Mg_{DSM3}$ (‰)	2SD	$\delta^{26}Mg_{DSM3}$ (‰)	2SD	n	Well
Post-injection monitoring well samples collected from HN-04								
12KGM08	09/02/2012	36	-0.43	0.05	-0.84	0.09	6	HN-04
12KGM11	16/02/2012	51	-0.45	0.06	-0.88	0.10	4	HN-04
12KGM19	27/02/2012	58	-0.49	0.05	-0.94	0.09	4	HN-04
12KGM25	08/03/2012	86	-0.49	0.05	-0.93	0.02	4	HN-04
12KGM33	26/03/2012	101	-0.48	0.04	-0.94	0.01	4	HN-04
12KGM44	18/04/2012	74	-0.54	0.05	-1.05	0.07	4	HN-04
12KGM49	04/05/2012	36	-0.48	0.06	-0.93	0.12	4	HN-04
12KGM60	30/05/2012	54	-0.52	0.06	-1.01	0.12	4	HN-04
12SOS01	08/06/2012	73	-0.53	0.07	-1.02	0.08	4	HN-04
12SOS09	17/07/2012	64	-0.52	0.07	-0.98	0.10	3	HN-04
12SOS15	31/07/2012	66	-0.57	0.04	-1.1	0.08	4	HN-04
12SOS21	14/08/2012	86	-0.51	0.03	-0.99	0.09	4	HN-04
12SOS28	28/08/2012	79	-0.67	0.06	-1.26	0.07	3	HN-04
12SOS34	24/09/2012	69	-0.57	0.04	-1.11	0.05	3	HN-04
12SOS39	29/10/2012	62	-0.59	0.04	-1.14	0.07	4	HN-04
13SOS01	07/01/2013	42	-0.64	0.07	-1.23	0.06	4	HN-04
13SOS10	16/04/2013	39	-0.69	0.07	-1.31	0.04	3	HN-04
13SOS17	10/06/2013	40	-0.62	0.01	-1.22	0.03	4	HN-04
14SOS11	08/06/2014		-0.69	0.06	-1.34	0.10	4	HN-04
Pre-injection samples taken from indicated shallow well.								
08HAA09	07/08/2008	180	-0.33	0.08	-0.64	0.11	5	HK-25
09HAA18	29/05/2010	175	-0.31	0.03	-0.57	0.06	3	HK-12
10HAA25	02/06/2010	226	-0.35	0.08	-0.69	0.13	3	HK-25
10HAA32	25/06/2010	169	-0.29	0.02	-0.59	0.02	2	HK-13
reference materials								
IAPSO seawater (batch a)			-0.47	0.04	-0.90	0.08	8	
IAPSO seawater (batch b)			-0.45	0.05	-0.88	0.08	4	
IAPSO seawater *mean (batch a & b)*			*-0.46*	*0.04*	*-0.90*	*0.08*	*12*	
seawater (reference value)[a]			*-0.43*	*0.06*	*-0.83*	*0.09*		
Cambridge-1			-1.35	0.06	-2.62	0.10	21	
Cambridge-1 *(reference value)*[a]			-1.34	0.03	-2.61	0.05		

[a] Published reference values are from compilations by Pogge von Strandmann et al. (2011), An and Huang (2014), Foster et al. (2010), Ling et al. (2011) and references therein.

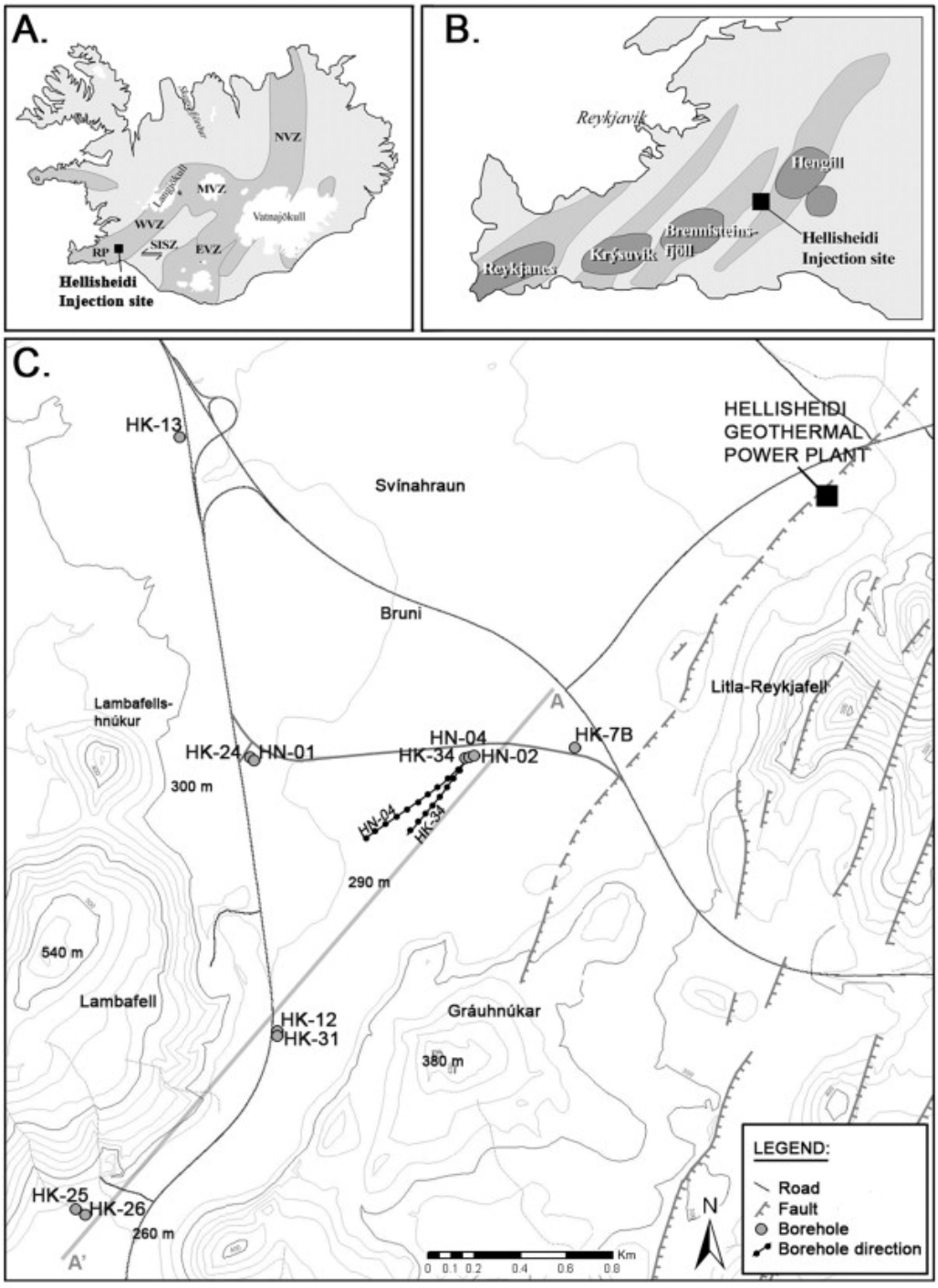

868
869
870 **Figure 1.**

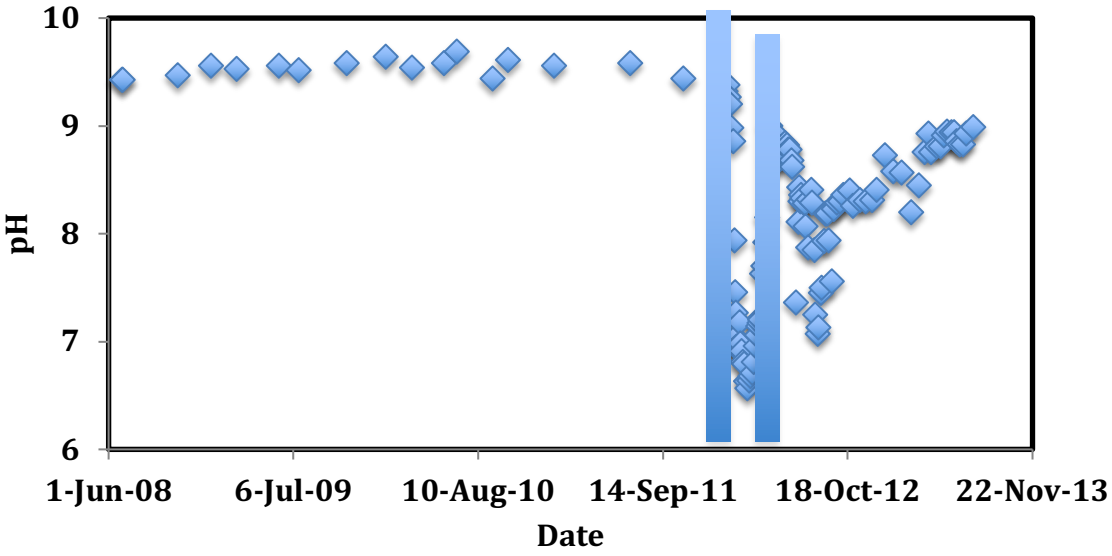

871

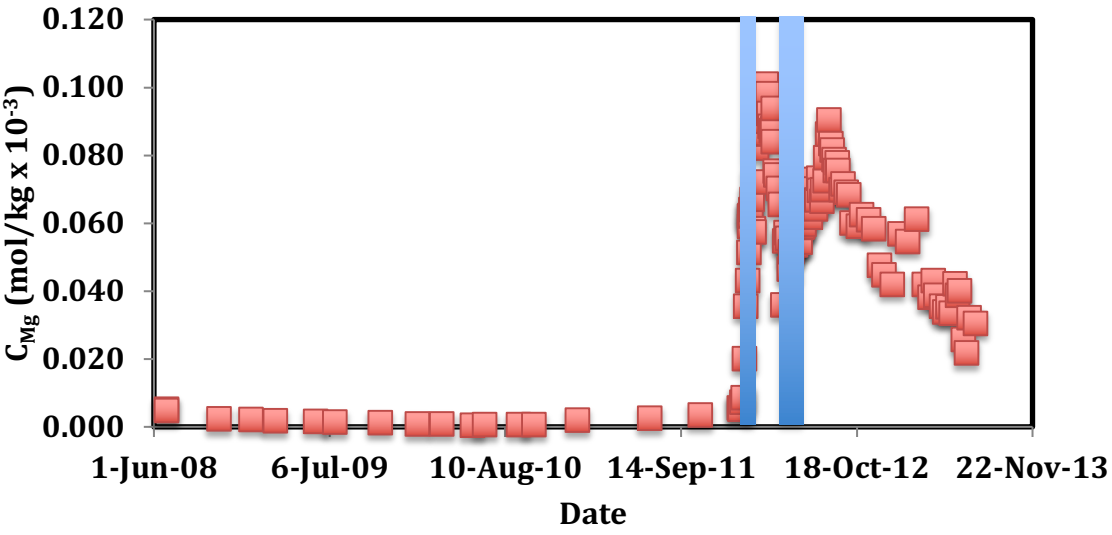

872

873 **Figure 2.**

874

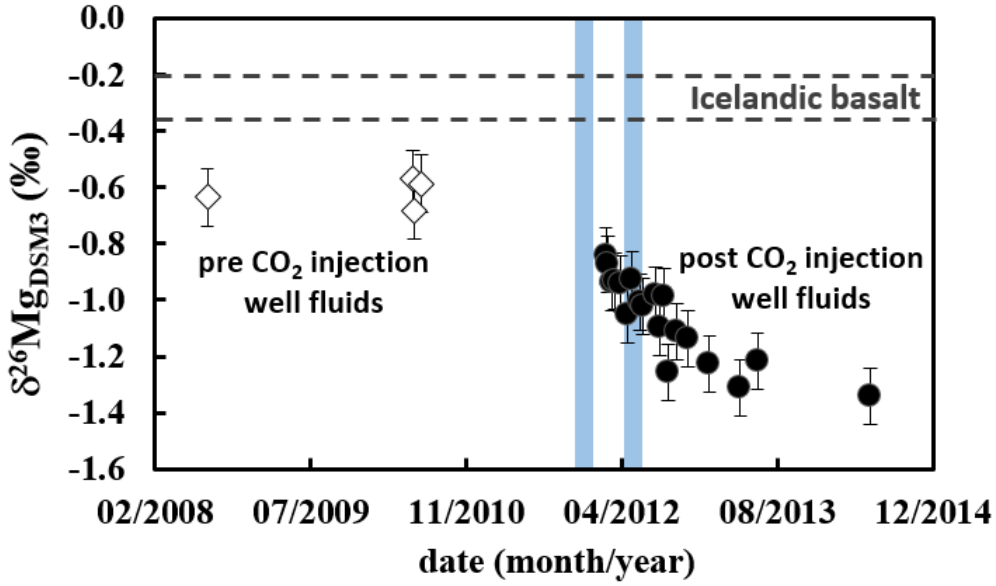
0.0
-0.2
-0.4
-0.6
-0.8
-1.0
-1.2
-1.4
-1.6
δ26MgDSM3 (‰)
Icelandic basalt
pre CO2 injection well fluids
post CO2 injection well fluids
02/2008
07/2009
11/2010
04/2012
08/2013
12/2014
date (month/year)

Figure 3.

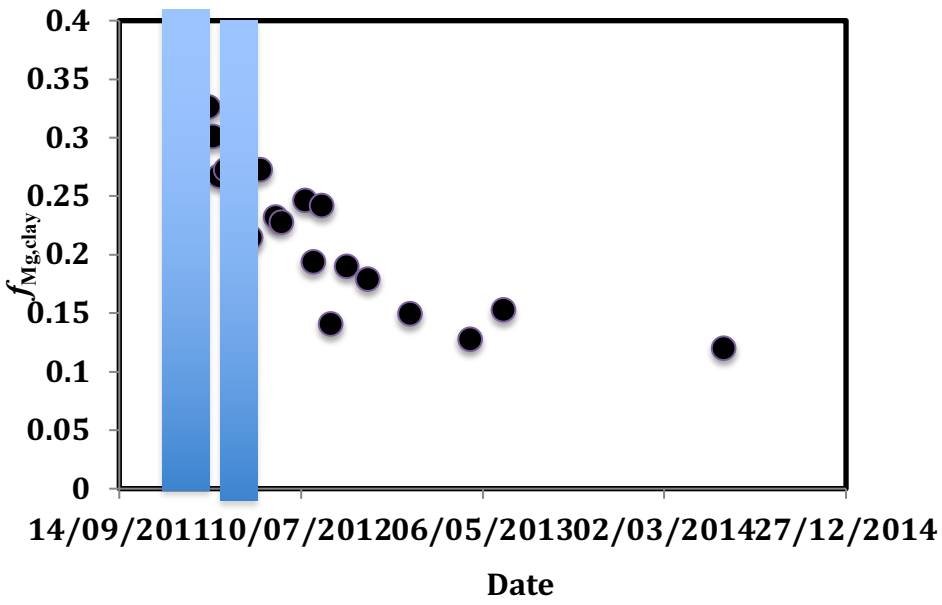

879

880 **Figure 4.**

881
882
883